ELEKTROTEHNIŠKI VESTNIK 88(5): 255-266, 2021
ORIGINAL SCIENTIFIC PAPER

Numerical Simulation of Polluting Particles' Trajectory Inside an Electrostatic Precipitator of Multi-Wire-to-Plate Electrodes

Imene Oualid, Samir Flazi, Naima Oussalah, Nacera Naoui, Habib Benamar, Amine Boudghene Stambouli

Electrical Engineering Laboratory of Oran, Faculty of Electrical Engineering, University of Sciences & Technology of Oran "Mohamed Boudiaf" USTO-MB, El Mouar BP 1505, Bir El Djir 31000, Oran, Algeria
E-mail Adresse: imene.oualid@univ-usto.dz

Abstract. The purpose of this article is to study the trajectory of air polluting particles in an electrostatic multiwire-plate precipitator at certain geometrical, electrical, and granular parameters which considerably affect the particle behavior when subjected to electrical, drag and gravitational forces. In the main part of the paper, the particles' trajectory and deposition along the ESP channel is modelled. Multiple 3D simulations are made using a Comsol Multiphysics Software to visualize the particles trajectory by including the necessary physical phenomena that occur inside the system obtained by using their adequate equations to set-up a consistent model to investigate the particles' tracking. The results of a non- uniform electric field are displayed as curves, and the particles' trajectory and deposition addressed in the literature are reported and discussed.

Keywords: particle trajectory, particle deposit, electrostatic precipitator, numerical modeling, 3D simulation.

Numerična simulacija krivulje poti onesnaževalnih delcev znotraj elektrostatičnega filtra

Namen članka je proučiti krivuljo poti delcev, ki onesnažujejo zrak v elektrostatičnem večžičnem situ ob določenih geometrijskih, električnih in zrnatih parametrih, ki pomembno vplivajo na obnašanje delcev, ko so izpostavljeni električnim, uporovnim in gravitacijskim silam. V glavnem delu prispevka sta modelirana krivulja in odlaganje delcev vzdolž kanala ESP. Več simulacij v prostoru 3D je izvedenih s programsko opremo Comsol Multiphysics za vizualizacijo poti delcev z vključitvijo fizikalnih pojavov, ki se pojavljajo v sistemu. Predstavljeni so rezultati vpliva neenakomernega električnega polja na krivuljo poti delcev.

1 INTRODUCTION

During this decade, several well-known international organizations, associations [1] and prestigious universities have all mobilized their research laboratories for long-term studies dedicated solely to air pollution, in order to evaluate its impact on the human life and how to deal with this kind of the phenomenon.

Given the extent of the danger of the air pollution, it is classified as the fourth triggering factor of premature death according to WHO statistics [2]. Despite being invisible to the naked eye, it is always ubiquitous in the atmosphere at different concentrations and in several forms depending on the region's sector of activity. Often, it comes from two types of activities, either resulting from natural phenomena or from human activities [3,4] which are generally the main contributors to this pollution [4] since they are still in full expansion.

It is no longer necessary to demonstrate the innumerable direct and indirect effects of the airborne pollution on public health [5,6]; it has been observed that children and the elderly are the most vulnerable people [7] in society affected by such pollution, taking into consideration the duration of exposure, whether it is short or long term [5,6].

Among the major sources of the air pollutants, the suspended particles matters (SPM) are the main sources of concern due to their impact on health, particularly at the cardiovascular and respiratory levels [8]. The United States Environmental Protection Agency (US EPA) classifies them as solid particles and divides them into three types: coarse, fine, and ultrafine particles [9]. They can travel for miles and stay in the air for hours or a couple of days [9] depending on their diameter.

In order to reduce their level in the air, several novel filtration methods [10] are still being proposed. Among them, a prominent position is held by the electrostatic precipitators [11], which have been widely used since the turn of the century. They can be found in heavy industry, waste incineration units, energy production, as well as at home or workplaces, because they can only limit the spread of polluting particles which come from a closed enclosure or a well-defined point source, as opposed to an open space.

The most basic setup consists of a stack of very fine wires in front of a metal plate that is spaced a few centimeters apart and has two operational zones: one for ionization and the other for collection.

Received 10 May 2021
Accepted 8 November 2021

Electrostatic precipitation is based on the electrostatic attraction principle. When dust-laden air enters the device, and close to the wires, the particles are then exposed to an ionizing field, which electrically charges the particles by giving them a polarity. When these ionized particles reach the collection plate, they are captured and powerfully retained by an electrostatic field of reverse polarity. They are periodically removed by simple routine maintenance operations, and the air comes out of the device purified and is almost rid of about 90% to 98% of these solid particles it contained because ithas the particularity of imprisoning particles of all micronic and submicronic sizes at each passage. Throughout the filtration process, particles charging and collection are done simultaneously.

As a result, knowing the trajectory of polluting particles as they enter the air filter attests to be a significant perspective in recognizing the primordial factors that have a direct impact on the deviation or not of these particles. This way, we'll know which element to focus on next in order to improve the filter's efficiency. Modeling all of the necessary phenomena governing within the pollution-control device appearsto be the best tool for clarifying assumptions through equations solved using the finite-element method, which we'll go over in more detail later.

Visualizing the pollutant particles streaming inside the ESP channel over one of its cross-sections seems to be a better way to determine the most affecting factors in deflecting and trapping these polluting particles.

2 NUMERICAL MODELING

In this section, we provide an overview of the essential considerations in modeling motion of pollutant particles on the entire electrostatic precipitator channel. This part describes the following steps for the simulation set-up. First of all, we define the geometry and then include the appropriate physics necessary for our investigation.

2.1 Computational Model Description

The modeling geometry is a simplified 3D configuration, (Fig. 1). It is a vertical channel with a multiple of identical conductors, all aligned on the same plane, ranging from **1** to **13**, so as the HV electrodes with a radius of value ***Rw*** that are held at fixed voltage ***Vapp***, and the whole is placed in parallel to a rounded planar plate at distance ***He***, with curvature ***e*** at the ends to avoid the appearance of the maximum of the electric field in these corners during our simulations. The wires are separated from each other at value ***k***, and the first wire is placed at distance ***i*** away from the inlet where the particles are injected, and are fixed on both sides by two plexiglass plates of thickness ***ep***, and the two other sides are considered as openings used as an inlet where the particles are fed through it, and one outlet where a clean air comes out from it separated by a long channel containing a carrier airflow considered as a neutral background gas.

As the particles pass through the long channel, they are mixed together with air and are subjected to a non-uniform electric field at an ambient pressure and the temperature of 20°C.

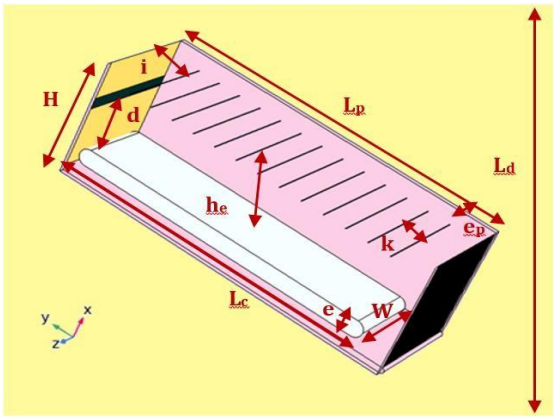

Figure 1. Presentation of a 3D geometrical model, including all dimensions of the related subdomains.

The model uses a multitude of wires next to a plate, but other geometries are possible. The proposed structure allow the particles to be seen from different angles, which can be accomplished by rotating it.

In Table 1, the values used to dimension the simulation domain are listed as follows:

Table 1. Constant geometric values and physical parameters for the simulating model.

Symbol	Value	Description
L [cm]	27,0	Length of the collecting plate
W [cm]	10,0	Width of the collecting plate
e [cm]	1,5	Thickness of the collecting plate
R_W [mm]	0,3	Radius of the wire
he [cm]	7,0	Distance between wires and the collecting plate
k [cm]	2,0	Inter-electrode distance
i [cm]	2,5	Distance from the entrance till the first electrode
d [cm]	2-6	Entrance level of injecting polluting particles
L_P [cm]	30,0	Length of the Plexiglas plates
e_P [cm]	0,5	Thickness of the Plexiglas plates
H [cm]	10,0	Height of the Plexiglas plates
L_d [cm]	150,0	Length of the computational domain
V_{app} [kV]	20-30	DC applied voltage
V_0 [m/s]	0,0	Air velocity
d_P [µm]	10-90	Particles' size distribution

Inside this transparent shell, there are non-transparent particles whose physical properties in a free space are crucial to be known for the ESP to operate perfectly by preventing the particles from escaping and getting stuck on the flat plate.

The model considers all the injected particles as elastic and small with diameter d_P of the micrometers order. They are assumed to be sperical, compact and concentrated, and are modeled as point particles.

All injected particulate matters are initially released uniformly from the ESP's entrance surface at t=0 s in the standing air flow, with all initial velocity components zero.

Table 2 lists the properties of the particles used in the model [12,13].

Table 2. Basic characterisation of the sample particles used during the numerical simulation.

Particles sample	Density	Dielectric constant
Lime [kg/m^3]	640,0	2,5
Portland cement [kg/m^3]	1506,0	2,5
Brick fire clay [kg/m^3]	2403,0	2,8
Concrete gravel [kg/m^3]	2403,0	4,5
Porcelain [kg/m^3]	2403,0	7,0

2.2 Included Physics Interfaces

For the needs of the study, the below three types of physical interfaces and features given by these three modules are used. They are tested and their suitability is discussed, and which are the following:

- Electrostatics module.
- Computational fluid dynamics module.
- Charged particle tracing module.

In this model, we first solve the two primary studies. Both Electrostatics and Fluid Flow are simultaneously computed using a stationary study and, in the second step, we set up the charged particles' movement study in a time-dependent solver. This is done by coupling a temporal study step for computing the particles trajectory to a steady- state study for calculating electric potential, electric field and the fluid velocity field.

Finally, the elaborated simulations are achieved to solve the model several times using a different set of factors each time.

2.2.1 Electrostatics module

To solve the electrostatics problem, we solve Gauss's law and the governing equations for the electric field in space between electrodes in the 3D channel given in [14,15]:

$$\nabla \cdot D = \rho_V \tag{1}$$

$$E = -\nabla V \tag{2}$$

Where: D is the electric displacement (C/m^2), ρ_v is the volume charge density (C/m^3), E is the electric field strength (V/m) and V is the electrostatic potential (V).

2.2.2 Fluid flow module

The fluid flow motion is governed by a set of the Reynolds-averaged Navier-Stokes (RANS) equations together with the continuity equation for standard laminar incompressible flow, one of the most frequently used laminar models in computational fluid dynamics. The laminar model introduces dependent variables as follows [15,16]:

$$\rho(\mu \cdot \nabla)u = -\nabla p + \mu\nabla^2 u + F \tag{3}$$

$$\nabla \cdot u = 0 \tag{4}$$

Where: ρ is the air density (kg/m^3), u is the air velocity (m/s), p is gas pressure (Pa), μ is the dynamic viscosity of the air (Pa.s) and F is the force acting on the gas (N).

2.2.3 Charged particles' trajectory module

The particles' motion equation is solved in one way. First the forces are induced in the model and are computed using the Particle Tracing Interface, which uses a continuum model in which the position is discretized using a finite element mesh in the modeling domain. The equation governing the evolution of the trajectory of particles in stagnant fluid is described by the Newton's second law, and it can be expressed as [17]:

$$\frac{(m_p v)}{dt} = F_e + F_D + F_G \tag{5}$$

The total force acting on the particles in a stagnant fluid under non-uniform electric field comprises a large number of physical phenomena but after some simplifications, it can be said that the following forces are the principal affecting the path of these rigid dust particles in ESP and which are: electrostatic force, viscous drag of the medium and gravity.

In this model, the electric force is assumed to be the dominant factor in determining the perturbed particles trajectory.

- Electrostatic force: if charged particles are placed in a non-uniform electric field E, they are subjected to a continuous electric force given by the following expression [14]:

$$F_e = ZeE_S \tag{6}$$

Where: e is the elementary charge (C), Z (dimensionless) is the particles charge number and E_S is the electric field strength (V/m).

- Mechanisms of particles' charging

Diffusion charging occurs when ions subjected to a random Brownian motion collide with and adhere to particles' surface. The diffusion charging mechanism is given in the following form [18,19]:

$$n_d = \frac{2\pi\varepsilon_0 d_P k_B T}{e^2} \ln\left(1 + \frac{c_i d_P e^2 N_i t}{8\varepsilon_0 k_B T}\right) \quad (7)$$

Field charging occurs when ions are carried by an external electric field to collide with and adhere to the surface of particles. The field charging mechanism is obtained from the following equation [18,19]:

$$n_f = \left(\frac{3\varepsilon_r d_P^2}{\varepsilon_r + 2}\right).\left(\frac{E_S \pi\varepsilon_0 d_P^2}{e}\right).\left(\frac{\pi e Z_i N_i t}{4\pi\varepsilon_0 + \pi e Z_i N_i t}\right) \quad (8)$$

Where: E_s is the electric field strength (V/m), ε_o is the vacuum permittivity ($C^2/N.m^2$), ε_p is the permittivity of the particle, d_p is the particle diameter (µm), k_B is the Boltzmann constant, T is the temperature (°K), e is the elementary charge (C), c_i is the mean thermal velocity of the ions (m/s), N_i is the concentration of ions ($1/m^3$) and Z_i is the electrical ion mobility ($m^2/V.s$).

The total charge of dust particles is experimentally demonstrated that it can be calculated with a practically sufficient accuracy as a sum of diffusion charge (7) and field charge (8) [20]:

$$n_t = n_d + n_f \quad (9)$$

- Drag force: the viscous drag force is appropriate to include in the model since the fluid in the straight channel is stagnant and the particles' speed is low. Furthermore, by treating the chaotic aspect of laminar flow in a statistical sense, the RANS equations permit stationary solutions to fluid flow problems. The particles experience a drag force given by the Stokes' law and is defined as follows [20]:

$$F_D = \left(\frac{1}{\tau_P}\right).m_P.(u - v) \quad (10)$$

The particle relaxation time is the time required for a particle.

$$\tau_P = \frac{\rho_P \cdot d_P^2}{18\mu} \quad (11)$$

Where: m_p is the particle mass (kg), d_p is the particle diameter (µm), v is the air velocity (m/s), μ is the air kinematic viscosity (m/s^2), ρ_p is the particle density (kg/m^3).

- Gravity force: since the device is placed vertically then the inclusion of the gravitation term is justified and the gravity force is calculated via the formula [17]:

$$F_G = m_P.g.\left(\frac{\rho_P - \rho}{\rho_P}\right) \quad (12)$$

Where: g is the acceleration gravity (m/s^2).

The condition to mention the right particles' diameter is also necessary for all the forces to be physically correct.

In this part, we neglect particles interaction since they are moving in a standing fluid, so less collision happening.

2.3 Boundary conditions settings

Particles are set to freeze on the solid walls but they disappear or pass through as long as the system is an open boundary.

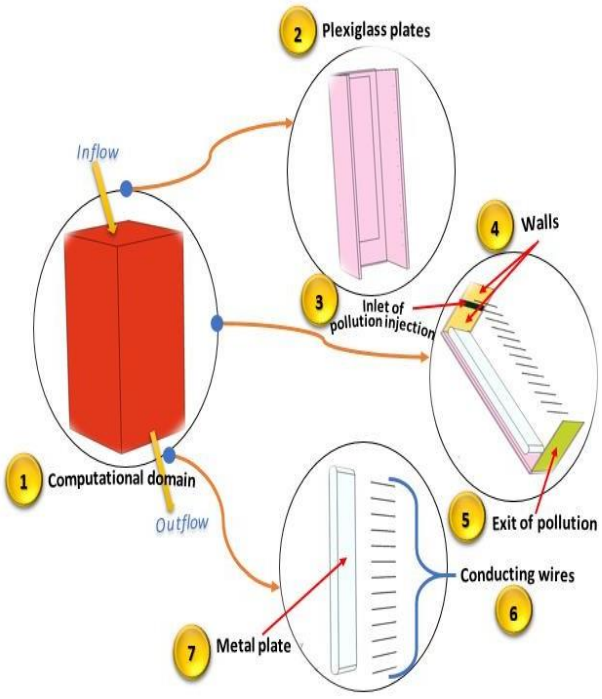

Figure 2. Divided subdomains with their specified boundary conditions.

In Table 3, we summarize the appropriate initial and boundary conditions for each physical interface.

Table 3. Summary of the initial & boundary conditions applied to the subdomains of the numerical model in each physical interface.

Modules / Domains or Boundaries	Electrostatics	Fluid flow	Charged particles' trajectory
Domain 1	Zero charge $n \cdot D = 0$	Inlet: Inflow $u_0 = u_y$ & Outlet: Outflow $p_0 = 0Pa$	Outlet Particles will freeze
Domain 2	Charge conservation $\nabla \cdot (\varepsilon_0 \varepsilon_r E) = \rho_v$		Particles will freeze
Domain 3			$N = N_P$ $v = u$
Domain 4			Walls: pass through
Domain 5			Particles will freeze
Domain 6	$V_0 = V_{app}$		Particles will bounce
Domain 7	Ground $V = 0$		Particles will stick up Particle Counter

3 SIMULATION RESULTS & DISCUSSION

The factors to study their impact on the trajectory of polluting particles are developed below. Simulation results show the several forms of representation of the trajectory taken by the particles within ESP and the way of the particles' deposition in each simulation is performed.

After several iterations, the model provides a solution for the particles' trajectory.

3.1 Geometrical aspects

In this section, we deal with parameters that are related to the geometric view of the device.

3.1.1 Entrance level of the polluting particles

In this part, we want to know the impact of the entry level of pollution on the shape of its trajectory inside the device. The entrance of pollution is distant at three lengths from the collection plate d=2, 4 and 6 cm.

The simulations below are carried out under the following conditions: V_{app}=30 kV, d_p=90 µm, ρ_p=1506 kg/m^3, ε_r=2.5 and N_p=30 injected particles at t=0s with only one HV electrode placed in the entry of ESP and we vary the level gate admission of the injected particles distanced from the collection plate.

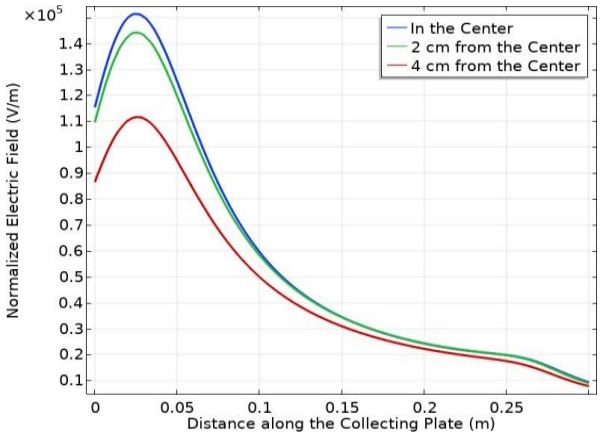

Figure 3. Calculated value of the electric field strength as a function of the distance along the collecting plate at three different locations for d=2 cm.

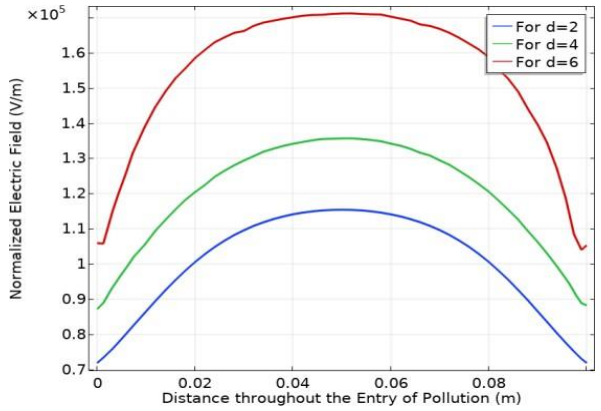

Figure 4. Normalized electric field through the entrance of the polluting particles at different levels of injection relatively measured from the collection plate.

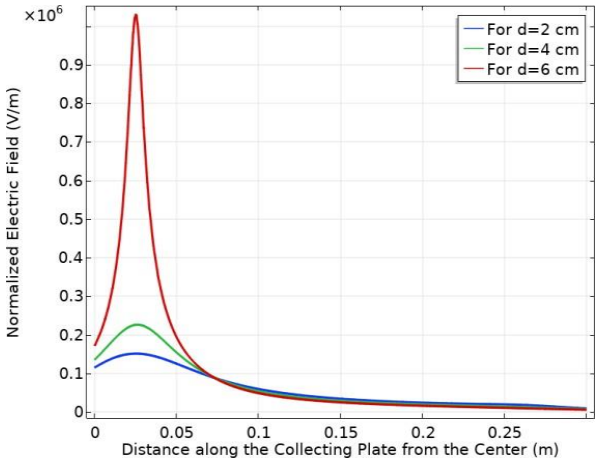

Figure 5. Calculated value of the electric field strength along the distance of the collection plate for three input levels of pollution.

Through Fig. 3, we clearly see for the curve from the center in comparison with the one close to the wall, moving away from the center towards the ends, the value of the electric field decreases considerably of the order of 40 kV/m this decline is only seen around the active zone (in the vicinity of the high voltage electrode) and this explains why the deposit is done well before in the center than near the walls (see Fig. 6.a).

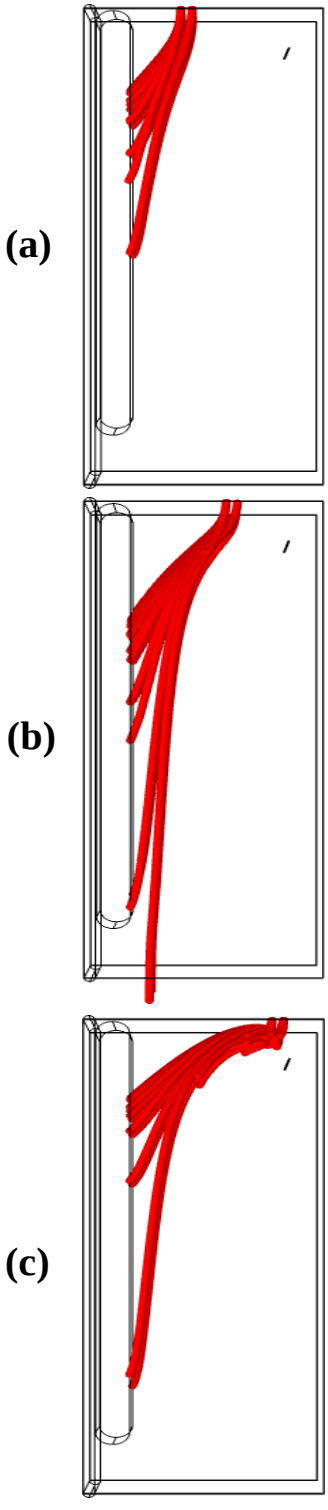

Figure 6. Tracing the trajectory of charged particles inside the system for (a) d=2 cm, (b) d=4 cm and (c) d=6 cm.

In the three obtained presentations of the particles' trajectory (see Fig. 6), almost all of the charged particles are deflected to the collecting plate, however the difference between these three demonstrations is that the more we move the entrance away from the plate the more the step becomes important which makes a long traveled distance by the particles to reach the plate even the curves showing the values of the electric field strength throughout the input as well as along the plate (see Fig. 4 & 5) explain that the more we back off further the input from the collecting plate the more the impact of the electric field on these particles becomes more significant and therefore there is a dilemma between the positioning of the particles and the electric field's value to get finally a reduced distance to cross.

3.1.2 Discharge electrode positioning

In this part, a brief investigation is made concerning the impact of the high voltage electrode's position on the particles' movement within the system.

The simulations below are carried out under the following conditions: V_{app}=30 kV, d_p=90 µm, ρ_p=1506 kg/m^3, ε_r=2.5, d=4 cm and N_p=30 injected particles at t=0s with only one HV ionizing electrode placed inside ESP and we change its position.

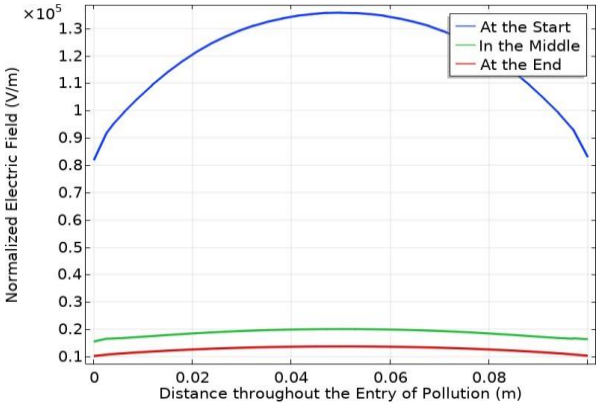

Figure 7. Normalized electric field through the entrance of the polluting particles for different position of the HV electrode.

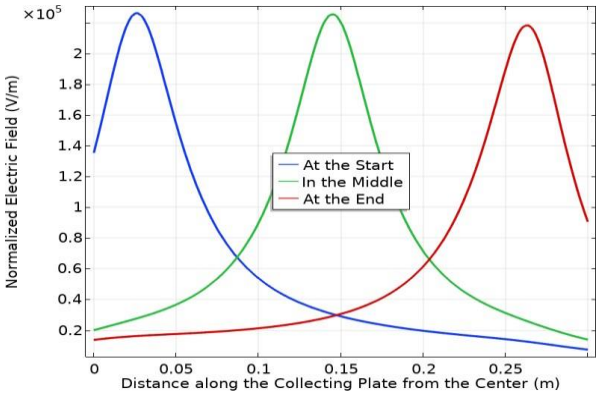

Figure 8. Calculated value of the electric field strength along the distance of the collection plate for different positions of the HV electrode.

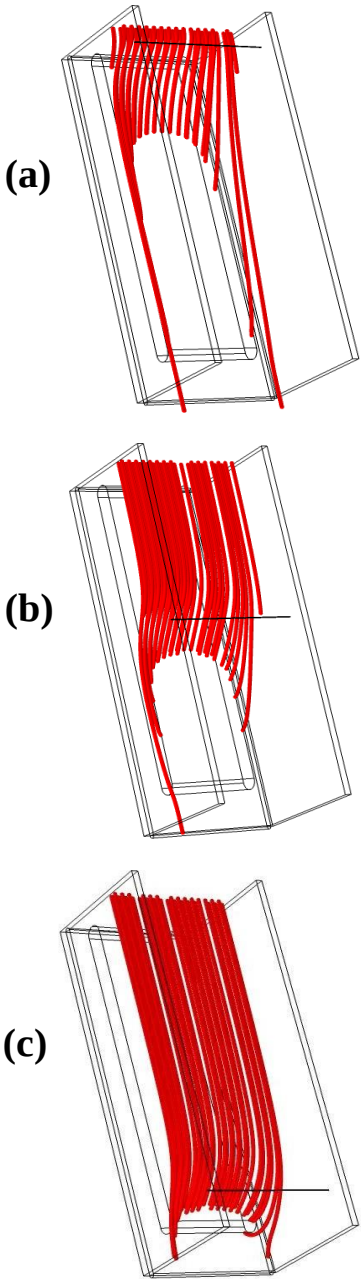

Figure 9. Tracing the trajectory of charged particles inside the system where the HV electrode is positioned (a) at the start, (b) in the middle and (c) at the end.

Fig. 9, shows that each calculated trajectory represents a continuous stream of particles. In Fig. 9.a, if the HV electrode is placed at the entrance of the supplying pollution, the particles are directly going to be deflected towards the plane plate and for those which are closer to the walls tend to fall down further than those situated in the middle of the channel. This is the reason why we obtain an oval shape deposit from the interior and for the particles injected near the walls are directly pushed towards them. By moving the HV electrode to the center in Fig. 9.b, all particles take a straight and rectilinear path, but as they approach near the wire, they bend quickly and for the ones near the walls move more further away as in Fig. 9.c, the curvature is even smaller so that some particles close to the walls escape out of the system.

In Fig. 8, although the shape of the curve and also the maximum value of the electric field reach through the collecting plate for the three positions of the HV electrode is the same everywhere, the glaring difference is observed in Fig. 7, for the curves of the electric field along the entry of the pollution. In the case of an electrode located in the beginning of the system, it is 7 times greater than those placed either in the middle or at the end and this is the reason why we obtain the particles' path as represented in Fig. 9.

3.1.3 Total number of corona electrodes

In this part, we study the impact of adding HV electrodes on the path taken by these particles.

The simulations below are carried out under the following conditions: V_{app}=30 kV, d_p=90 µm, ρ_p=1506 kg/m^3, ε_r=2.5 and N_p=30 injected particles at t=0s with d=4 and we vary the number of HV electrodes.

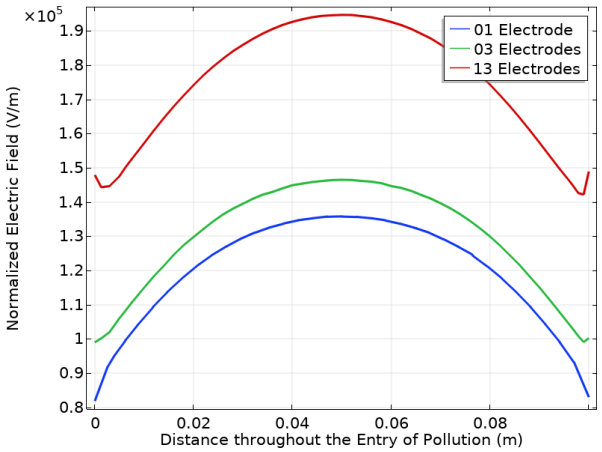

Figure 10. Normalized electric field throughout the entrance of the polluting particles for a different number of the electrodes added.

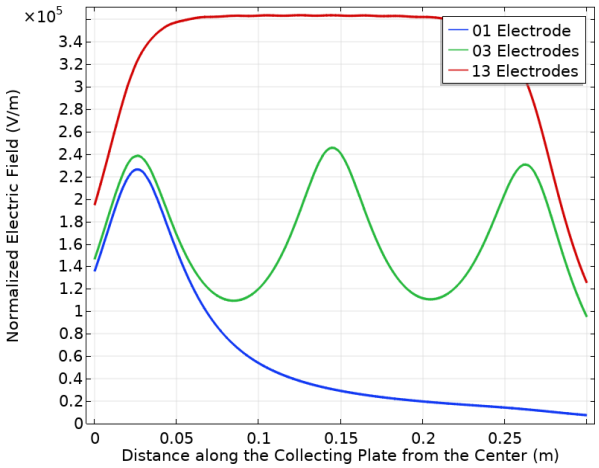

Figure 11. Calculated value of the electric field strength along the distance of the collection plate for a different number of the HV electrodes added.

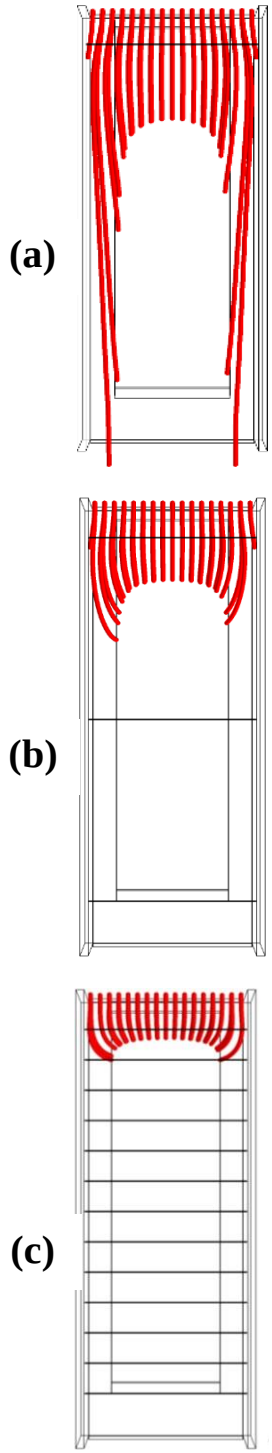

Figure 12. Projection of the polluting particles' trajectory on the z-y plane with (a) a single HV electrode, (b) three HV electrodes and (c) 13 HV electrodes placed in the implemention.

During the simulations depicted in Fig. 12, we observe that the more HV electrodes are placed in the system, the faster the particles are deflected, and therefore the deposition will take place well in advance and this result can be justified through Fig. 10 which shows that the more we add electrodes plus the value of the electric field increases considerably and that makes a huge difference between its value for 13 electrodes relative to 3 or 1 electrode and also because of the shape of the electric field's curve for 13 electrodes, takes on a homogeneous and straight appearance which also means that the electric field's lines are accentuated inward between the wires and the plate along the Y-axis instead of being inhomogeneous and dispersed throughout the domain in the case of 3 and 1 electrode in Fig. 11.

3.2 Electrical aspects

In this part, we deal with parameters that are related to the electrical view of the system.

3.2.1 Supplied DC high voltage

In this section, we study the effect of the applied voltage variation on the particles' track.

The simulations below are carried out under the following conditions: d_p=90 µm, ρ_p=1506 kg/m^3, ε_r=2.5 and N_p=30 injected particles at t=0s for d=4 cm, with 13 HV electrodes placed within the system, and we switch the applied voltage to a value for each simulation.

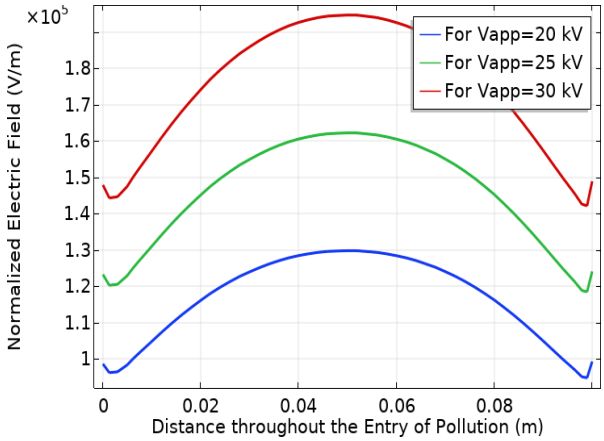

Figure 13. Normalized electric field through the entrance of the polluting particles for different applied voltages.

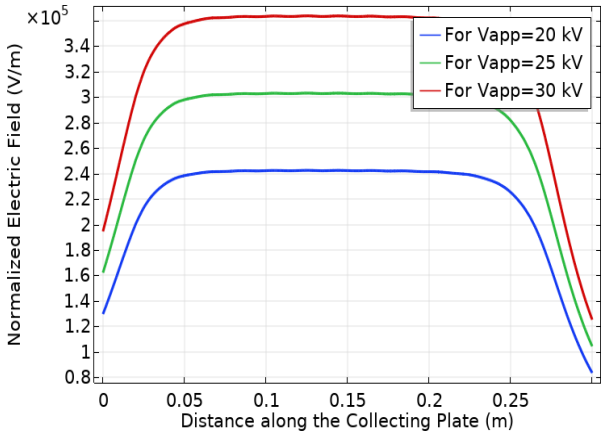

Figure 14. Calculated value of the electric field strength along the distance of the collecting plate for different applied voltages.

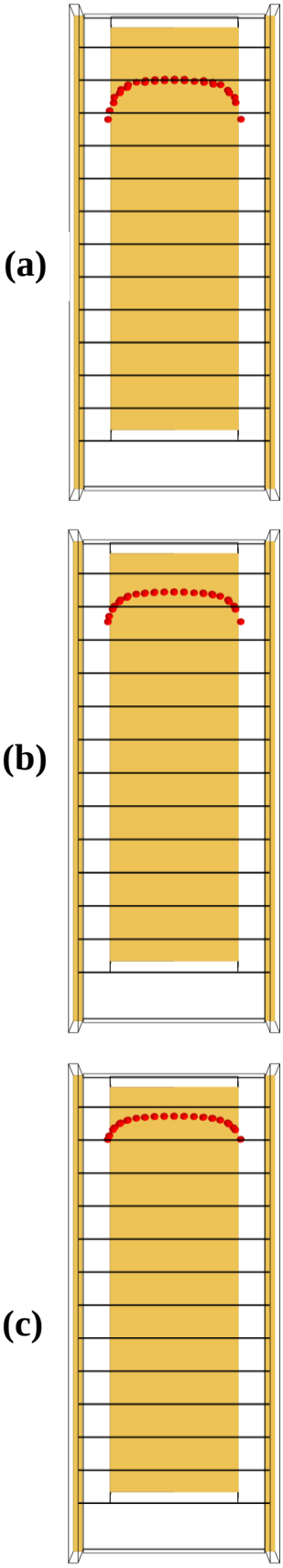

Figure 15. Predicted particles' deposition along the configuration for an equivalent applied voltage of (a) Vapp=20 kV, (b) Vapp=25 kV and (c) Vapp=30 kV.

In Fig. 15, for each run, different random depositions are generated and we perceive that the higher the applied voltage is, the earlier the precipitation comes about compared to two others. Moreover, by elevating the voltage there would be no greater variance between the particles settled at the center and those which are closer to the walls. Thus, all of this is reflected through the curves of the electric field in Figs. 13 & 14. The more the exerted voltage is multiplied, the more the value of the electric field rises and the charging is done better in a large quantity for particles and the accumulation is made closer towards the input of the device.

3.2.2 Dielectric constant of the polluting particles

In this section, we study the impact of the dielectric constant variation on the particles' orientation.

The simulations below are carried out under the following conditions: d_p=45 µm, ρ_p=2400 kg/m^3 and N_p=30 are the injected particles at t=0s for d=4 cm and with a single HV electrode placed close to the outlet. The particles' permittivity is changed.

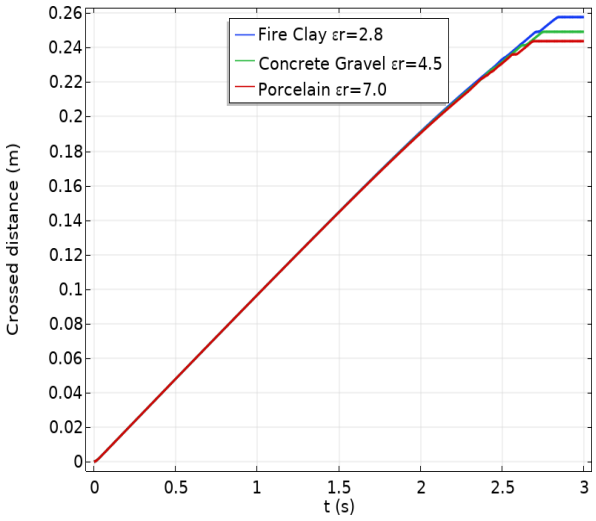

Figure 16. Maximum distance reached by the particles have reached along the y coordinate over time for three types of permittivity.

The above graph shows that after the injection of the three types of pollution at the inlet of the system, they follow the same path and this is explained by the superposition of the three curves but arriving closer to the end of the plate, all the three categories of contaminating particles are deflected. The porcelain particles settle a little more in advance than the concrete, then comes the turn of the fire clay which is much closer to the exit.

The more we deal with the particles owning to a high permittivity, the shorter their path will be and the faster they move towards the plate.

Since the three samples of the pollutanting dust particles have different dielectric properties, so the value of this electric strength is different too.

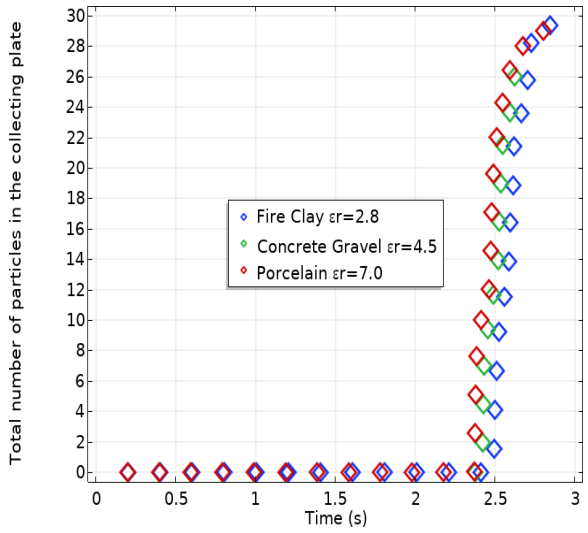

Figure 17. Total number of collected particles on the plane plate over time for three kinds of permittivity.

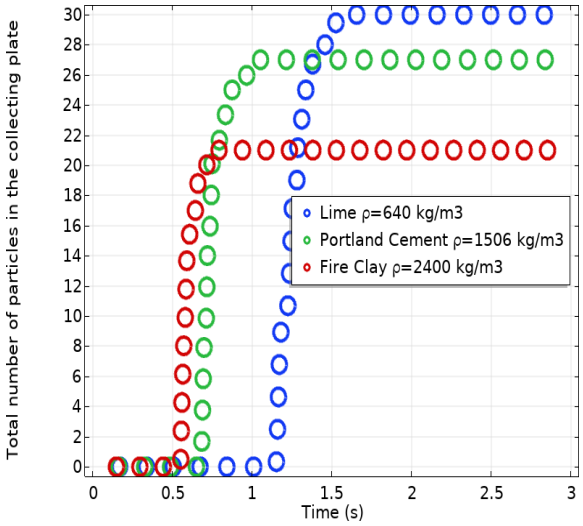

Figure 18. Total number of collected particles on the plane plate over time for three kinds of the particles' density.

In Fig. 17 above, we have three curves which represent the number of particles collected on the plate over time.

We note that the greater is the permittivity of the polluting particles, the more the deposition takes place a little bit earlier but still all the three graphics arrive at the same total number of accumulated particles on the metal plate.

3.3 Granular aspects

In this section, results related to the granular properties of the particles are given.

3.3.1 Polluting particles' density

The simulation is solved each time with a different particles' density.

The simulations below are carried out under the following conditions: V_{app}=30 kV, d_p=90 µm, ε_r=2.5 and N_p=30 injected particles at t=0s with only one HV electrode positioned in the middle of ESP, and we choose three varieties of particles with a different density.

The graph in Fig. 18, shows the number of particles deposited on the collecting plate as a function of time for various densities. We realize that the smaller is the density, the more quickly the solid particles migrate towards the collection plate, earlier than the others but on the other hand, if the density is high, the particles tend to come out of the system and we cannot collect the total number of particles initially emitted at the inlet, which is the case for the fire clay particles.

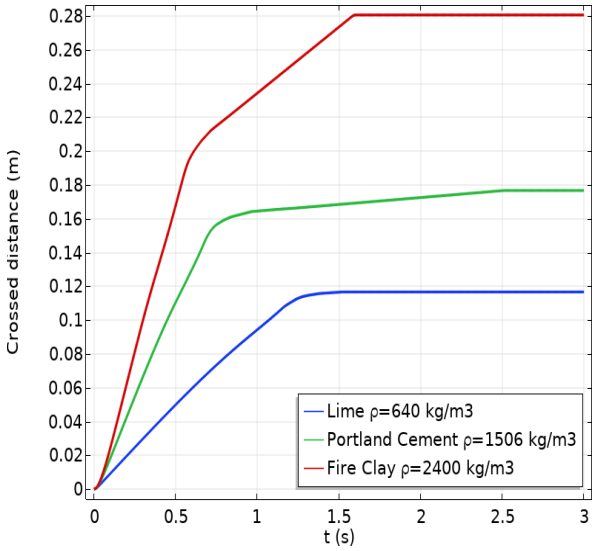

Figure 19. Maximum distance the particles reach along the y coordinate over time for three varieties of particles' density.

The graph shows that the more the density of particles increases, the more the traveled distance by particles is extended. The difference in positioning the lime and the portland cement particles is greater than that between the portland cement and the fire clay even though the density difference between the first and the second is the same as between the second and the third in the order of 800 kg/m^3.

The greater the density of particles is, the better the gravity force acts on them, and thus it will be more difficult to deflect them consistently to the collecting plate of the channel.

3.3.2 *Polluting particles' diameter*

In this section, we investigate the effect of modifying the molecules' diameter on their localization on the plate.

The simulations below are carried out under the following conditions: V_{app}=30 kV, Ne=3, ρ_p=1506 kg/m^3, ε_r=2.5 and N_p=30 injected particles at t=0s with only one HV electrode placed at the entry of ESP and we vary the diameter of the inserted particles.

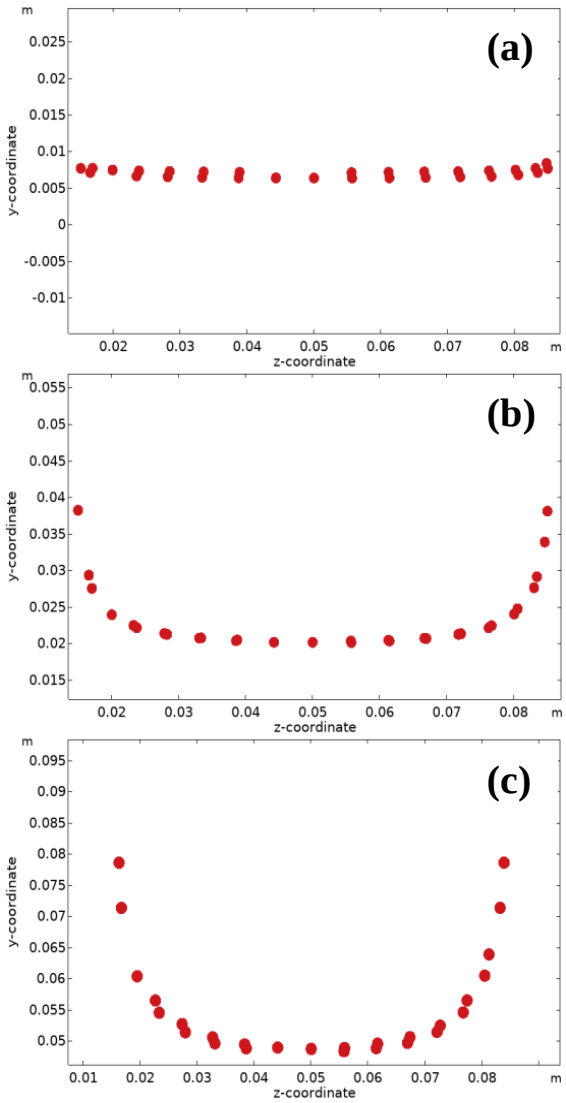

Figure 20. Snapshot of the final position of particles plotted according to their y and z coordinates for the following particles size (a) dp=10 µm, (b) dp=45 µm and (c) dp=90 µm.

In the above figures, the computed traces of the deposits' locating is shown in a map on the y-z plane. In each case, the particles' position is somewhat unlike but all cases agree with the results from solving the equation (5). We notice that by enlarging the size of the particles, they tend to move away in the direction of the exit and also the distance gap increases between the particles that are at the beginning and those that are in advance along the y axis. However, no change occurs according the z axis because all the particles are limited between 1.5 and 8.5 cm.

It is explained by the difference in the diameter, if we go for a bigger size, they will feel a larger electric strength than the other ones and so are deflected but this applies just for 10 to 45 µm and 90 µm. These particles have a sufficient inertia to cross a long distance in the fluid and this is mainly due to the gravitational force that just acts along the y axis by dragging them downwards.

4 CONCLUSION

Results of our simulations show the impact of changing each parameter, i.e. geometric, electrical and granular, on the trajectory of the polluting particles within the modeling domain. Our conclusions are the following:

a) Geometrically, the level of pollution injection, the location and the number of the electrodes used in our model importantly affect both the shape of the trajectory and the estimation of the traversed distance.

b) Electrically, the application of a high voltage significantly affects the propagation of the charged particles, and the disruption of the particles' trajectory manifests itself in the deposit's advancement or retreat relative to the system's input. On the other hand, the dielectric constant less affects their deviation than the other parameters. It does not prevent a new trajectory to be processed and studied to know its impact on the crossing distance.

c) Simulation of the granularity show to what extent the variation of granularity size and density affects the deposition and the positioning of dust particles on the plate.

As the diameter and density of the polluting particles are outside the range of human vision, the study makes it possible to determine the value at which forces are strong enough to drag the particles using the presented model. To further improve its stability and robustness, some other affecting parameters should be studied in the future.

ACKNOWLEDGEMENT

We would like to express our sincere gratitude to all the members of the Electrical Engineering Laboratory of Oran (LGEO).

REFERENCES

[1] Berkeley Library University of California online "Environmental Health: Organizations and Associations – environmental health resources", http://guides.lib.berkeley.edu/publichealth/envirohealth/or (Last updated 25.3.2021).

[2] Laura Tuck, Keith Hansen, Christopher Murray "The Cost of Air Pollution: Strengthening the Economic Case for Action", *World Bank Group IHME*, 2016.

[3] C. Pénard Morand, I. Annesi Maesano "Air pollution: from sources of emissions to health effects", *Breathe*, 1(2), 2004.

[4] WHO.Int online "Ambient air pollution: Pollutants", http://www.who.int/airpollution/ambient/pollutants/en/.

[5] Mark Li, Léo Mallat "Health impacts of air pollution", *SCOR Global Life Paper*, (42), 2018.
[6] Adel Ghorani Azam, Bamdad Riahi Zanjani, Mahdi Balali Mood "Effects of air pollution on human health and practical measures for prevention in Iran", *Journal of Research in Medical Sciences*, 2016.
[7] Marzia Simoni, Sandra Baldacci, Sara Maio, Sonia Cerrai, Giuseppe Sarno, Giovanni Viegi "Adverse effects of outdoor pollution in the elderly", *Journal of Thoracic Disease*, 7(1), page. 34-45, 2015.
[8] WHO "Health effects of particulate matter", *WHO regional office for Europe*, 2013.
[9] WHO "Health risks of particulate matter from long-range transboundary air pollution", *WHO Regional Office for Europe*, 2006.
[10] B.G. Miller "8-Particulate Formation and Control Technologies", J. Clean Coal Engineering Technology (Second Edition) Butterworth-Heinemann, 77(1), page. 419-465, 2017.
[11] J.H. Turner, P.A. Lawless, T. Yamamoto, D.W. Coy, J.D. McKenna, A.B. Nunn, G.P. Greiner, J.D. McKenna, W.M. Vatavuk "Chapter 3-Electrostatic Precipitators, Section 6-Particulate Matter Controls", *U.S. National (EPA)*, 1999.
[12] Simetric.co.uk online, "Density of materials", https://www.simetric.co.uk/si_materials.htm (Last modified 24.2.2016).
[13] Clipper Controls Inc online, "Dielectric Constant Values", https://www.clippercontrols.com/pages/Dielectric-Constant-Values.html#C .
[14] B. Benamar, E. Favre, A. Donnot and M.O. Rigo "Finite Element Solution for Ionized Fields in DC Electrostatic Precipitator", *Ein Comsol Users Proceedings*, 2007.
[15] Helena Nowakowska, Marcin Lackowski and Jerzy Mizeraczyk "Modelling of electrohydrodynamic (EHD) flow in a cylindrycal precipitator with eccentric wire electrode", *Przegląd Elektrotechniczny*, 2016.
[16] G.N. Sunil, Amaresh Dalal, Ganesh Natarajan "Computation of Flow Coupled with the Electic Field on Unstructured Grid", *Proceedings of the 5th International and 41st National Conference on FMFP*, 2014.
[17] Zhuangbo Feng, Zhengwei Long, Kazimierz Adamiak "A Critical Review of Models used in Numerical Simulation of Electrostatic Precipitators", *IAPGOS*, 2017.
[18] Antti Rostedt " Diffusion Charging-Based Aerosol Instrumentation: Design, Response Characterisation and Performance ", *Tampere University of Technology*, vol. 1527, 2018.
[19] Jeffery.S. Marshall, Shuiqing Li "8-Particle Interactions with Electric and Magnetic Fields", *Cambridge University Press*, pages. 223-255, 2018.
[20] Maria Jędrusik, Arkadiusz Świerczok Wroclaw "9-Design Efficiency of ESP", *Wroclaw University of Technology Poland*, 2012.

Imene Oualid got her master's degree in 2015 in Electrical Energy Techniques and since then she has been pursuing her doctoral studies in the field of plasmas and electrical discharges engineering. Her research field is mainly dedicated to the study of electrostatic filters.

Samir Flazi received the B.E degree in electrical engineering from Aleppo University in 1973 and then he completed his D.Eng. and D.E at Paul Sabatier University, in France, in 1981 and 1987 respectively. He started working at the University of Sciences & technology of Oran, in Algeria, since 1979 until he retired in 2020. He was a professor in the electrical engineering department and also a director of the high voltage laboratory. His research interests are flashover, pollution measurements, breakdown in front of a discharge and electrostatic application.

Naima Oussalah received her university applied studies diploma in 1997, the Ing. Diploma in 2000, the master degree in 2002 and Ph.D in January 2008, from the University A. Mira of Bejaia, Algeria. From 2002 to 2008, she was an Assistant lecturer at the university of A. Mira of Bejaia. Since October 2008 she teaches at the University of Sciences and Technology of Oran M. Boudiaf, Oran, Algeria where she obtained the Habilitation in December 2009. Her areas of work include partial discharges in power cables and corona simulation using the finite element method.

Nacera Naoui received the B.E and M.E degree in electrical engineering from university of Science and Technology of Oran, Algeria in 2002 and 2005 respectively. She is teacher-researcher at High voltage laboratory of the same university. Her research interests are flashover on the polluted insulator, conception of self-cleaning electrostatic air filter, fault localization for transmission lines.

Habib Benamar obtained his engineer's degree in June 1994 then his magister in electrical engineering in July 2005. From December 2005 till today, he is a teacher at the University of Sciences and Technology of Oran, where he taught several educational modules in the electrical engineering department. He currently holds the position of assistant professor and he is also a researcher in the electrical engineering laboratory of Oran (LGEO). His research area is mainly on electrostatic filters.

Amine Boudghene Stambouli graduated from the University of Sciences & Technology of Oran (USTO, Algeria) with an Engineering degree of Electronics in 1983 and then he completed his Master's degree in Modern Electronics in 1985 and his PhD studies in Optoelectronics in 1989 at the University of Nottingham in England. In 1995, He started working on High Field Electroluminescence and Optoelectronics at USTO. In 2002, he was promoted to full Professor of Optoelectronics and Material Science for Environment and Energy Applications at the Department of Electronics of USTO. In 2013, he was appointed as the Director of the Electrical Engineering Laboratory of Oran. Amine's current research projects include Photovoltaics, Fuel cells, Hybrid Systems, and Environment Impacts.